ELSEVIER

Journal of Non-Crystalline Solids 263&264 (2000) 228–239

JOURNAL OF NON-CRYSTALLINE SOLIDS

www.elsevier.com/locate/jnoncrysol

Surface tensile layer generation during thermal annealing of phosphate glass

J.S. Hayden [a,*], A.J. Marker III [a], T.I. Suratwala [b], J.H. Campbell [b]

[a] *Schott Glass Technologies, Inc., 400 York Avenue, Duryea, PA 18642, USA*
[b] *Lawrence Livermore National Laboratory, P.O. Box 808, Livermore, CA 94551, USA*

Abstract

Surface tensile layers (up to 20 MPa) are generated during thermal annealing of metaphosphate glass in ambient air. The surface tensile stress is caused by changes in properties of the phosphate glass, particularly the glass transition temperature and the coefficient of thermal expansion, due to the glass reaction with water vapor and diffusion of OH groups into the region just below the surface (<2 mm). An increase in the OH content of the glass from about 80 to 5000 ppmw causes a decrease in the glass transition temperature from 468 to 405°C and an increase in the linear thermal expansion coefficient from 12.9 to 14.2×10^{-6} K^{-1}. A mechanism for the generation of the tensile surface layer is proposed and simulated experimentally by fusion-bonding at 500°C two samples of the same composition but with OH contents that differ by up to 50×. The stresses in the annealed fusion-bonded samples are determined from measured stress birefringence. Peak tensile stresses calculated by finite element analysis agree with measured values to within 30%.

1. Introduction

Nd-doped meta-phosphate laser glasses are the preferred gain medium for use in high-peak-power lasers for fusion energy research [1,2]. Fusion lasers currently under construction [3,4] will have output energies of nearly 2 MJ and each requires more than 3000 slabs of laser glass; each slab is nearly $81\times46\times4$ cm^3 in size and contain approximately 15 l of glass. The phosphate glass slabs needed for these laser systems can be made by either discontinuous or continuous melting processes [1]. In either case, the glass exiting the melter system is formed into castings large enough to yield finished optics of the required size and shape; these castings are then thermally annealed [1].

Following thermal annealing, as-formed phosphate laser slabs are often observed to have surfaces with large tensile stresses. This is in contrast to most as-formed silicate glasses that exhibit compressive surface layers [5] after a similar annealing cycle. Tensile surfaces, in combination with available crack nucleation points, can result in the development of a network of shallow surface cracks. Surface cracks can become a production yield issue if they propagate and cause catastrophic fracture of processed glass.

The development of compressive surface stresses as a result of annealing, typically observed in silicate glasses, is well understood [5]. In brief, as the produced glass cools, a parabolic temperature

* Corresponding author. Tel.: +1-570 457 7485; fax: +1-570 457 6960.
E-mail address: jhayden@schottglasstech.com (J.S. Hayden).

0022-3093/00/$ - see front matter
PII: S0022-3093(99)00672-9

gradient is created through the glass with the surface temperature less than the interior. At temperatures above the glass transition temperature, T_g, stresses are relaxed by viscous flow. Once the glass cools below T_g, the thermal gradient through the glass causes a temporary stress with tension on the surface and compression in the interior simply because the surface has cooled more (i.e. shrunk more) than the interior. When the glass reaches room temperature, the thermal gradients are eventually removed and so are the temporary tensile stresses at the surface. The source of the residual surface compressive forces in silicate glasses can be traced to events near T_g. Specifically, at temperatures near T_g, the glass relaxes (i.e. undergoes viscous flow) to yield a reduction in some of the temporary stress that is generated by the cooling-induced thermal gradient through the glass. Subsequently, what remains in the glass at room temperature is a permanent stress that is equal and opposite to the temporary stress relaxation that occurred near T_g. The result is a surface under compression and the interior under tension [5].

In contrast to the above mechanism, the formation of a tensile surface layer observed in phosphate glasses is different and the elucidation of the mechanism for this tensile layer formation is the purpose of this study. We show that water vapor from the atmosphere diffuses into the surface of the formed glass and significantly alters the properties of the surface. The result is that the OH-containing glass near the surface shrinks more than the interior and a tensile surface layer develops.

In this paper, we first describe some of the properties of the tensile layer and surface fractures in annealed phosphate glass slabs. Then we propose a mechanism for the generation of a tensile layer on phosphate glass surfaces based on the different shrinkage characteristics of the surface and interior of the glass. To illustrate the mechanism, fused laminates are made of two metaphosphate glass plates with the same composition but different OH contents and the maximum stresses near the laminate interface are measured. These stresses are compared with those predicted by finite element analysis (FEA). Finally, we discuss how stresses can be reduced or eliminated in annealed glass slabs.

2. Properties of observed tensile layer and surface fractures

Laser glasses are typically formed into large slabs of a near-rectangular shape (approximately $100\times50\times6$ cm^3) by pouring into a steel mold at completion of the discontinuous melt process [1]. The casting is then placed, while still above T_g, into an annealing oven that is also at a temperature just above T_g. The glass is then annealed at a cooling rate of $\leqslant 30$°C/h producing a glass with a stress at room temperature of $\leqslant 2$ MPa allowing it to be cut, polished and inspected. This glass blank is then annealed again at a slower rate ($\sim$10–20°C/day) [1] to reduce stresses to a point that the birefringence is less than 5 nm/cm ($\leqslant 0.25$ MPa).

After the first annealing cycle, phosphate glass slabs often have cracks on the as-cast surfaces. Two types of crack patterns are frequently observed, which we term Type I and Type II cracks. Type I cracks, sometimes referred to as spider-web cracks because of their general appearance, cover nearly the entire top and side surfaces of castings. The areal density of cracks can vary and crack separation distances can be as small as a few millimeters. Also, Type I cracks rarely penetrate more than a few millimeters into the casting. The effected glass is normally removed in subsequent surface finishing (e.g. Blanchard grinding) and generally Type I cracking does not lead directly to catastrophic fracture.

Type II cracks are larger and often extend from the edges and sides of the casting into its center region and, on occasion, through the full casting thickness. Because Type II cracks penetrate a large fraction of the thickness of a casting, they make the product unusable.

Analysis of fractured glass surfaces, using a microscope equipped with polarizers and a compensating prism, indicates that there exists a surface tensile layer along the top, side, and to a lesser extent, the bottom surfaces of the phosphate glass castings. The magnitude of the stress varies, but in

many cases exceeds 20 MPa as determined from the stress birefringence near the glass surface.

Fractography analysis of the Type I and Type II cracks indicates that fracture origin is often small pits on the top surface of the castings [6], which are attributed to foreign material falling onto hot glass during or immediately after the castings operation. Fracture begins with the Type I crack pattern which is nucleated at these surface pits described above, but growth is limited to a shallow surface tensile region only a few mm in depth. Thermal gradients in the casting during subsequent annealing, handling and processing can then lead to propagation of Type I surface cracks into the much larger Type II fractures.

3. Experimental

3.1. Glass melt preparation

Six glass melts (labeled as glass samples A–F) having the same metaphosphate composition except with varying hydroxyl (OH) contents were used in this study. The base glass is a commercial laser glass (LG-770) [7] and has the composition (mol%): (58–62)P_2O_5–(6–10)Al_2O_3–(20–25)K_2O–(5–10)MgO and (0–2)Nd_2O_3. The composition is reported using ranges to account for volatile losses during melting, variations in Nd-doping (which depend on the intended laser application), batching variability and also to protect certain proprietary aspects of the composition. Note however, for the range of compositions shown above, the properties of the glass vary only slightly and do not affect the results of this study. For example, data reported by Campbell and Suratwala [2] show that for the glass properties important for this study (coefficient of thermal expansion, density, fracture toughness and Young's modulus), the variation is $<\pm 15\%$ over the composition range given above. Similarly, recent studies of phosphate glass manufacturing [1] show that the processing steps and conditions are nearly identical even though the product glasses have different compositions. Finally, and perhaps most important, a recent study of fracture growth in metaphosphate laser glasses shows that subcritical crack growth is relatively insensitive to small composition variations but much more dependent on the OH content in the glass and the water vapor content of the surrounding process atmosphere [8]. Therefore, we are confident that the results from this study are insensitive to the minor composition variations listed above.

All melts were prepared at 1250°C, cast into steel molds and annealed at 500°C for two hours, and then cooled to room temperature at about 30°C/h. Glass sample A is a production glass melt made using discontinuous melting [1]. This glass contains a low OH content (absorption at 3000 cm^{-1} of ~ 0.8 cm^{-1}; OH $\leqslant 100$ ppm). Glasses B–F were from 0.5 l melts prepared in inductively heated quartz crucibles using procedures described elsewhere [9]. The hydroxyl content in glasses B–F was varied by adjusting either the amount and duration of O_2 bubbling through the melt (0–0.5 l/min at STP) or the duration of the refining time (2.5–3.5 h), all of which decrease the hydroxyl content of the glass. Glass melts with larger hydroxyl content were generated by the direct addition of small amounts of water into the batch prior to melting (2–5 g H_2O/1000 g batch). Details of relationship of the H_2O content in the raw materials to the hydroxyl content in the glass, as well as the effect of processing parameters on the OH content in the glass, are described elsewhere [1].

3.2. OH concentration and concentration-profile measurements

Glass samples ($10\times 10\times 2$ mm^3) were cut from the exposed (top) surfaces of the melt glasses; the original exposed surface (10×10 mm^2 face) was untreated while the opposing surface was polished. The average OH concentration through the glass was determined from the absorption band at 3.333 μm (3000 cm^{-1}) using a FTIR spectrometer (Perkin–Elmer Spectrum 2000) operated in the transmission mode. The OH concentration is expressed in terms of the OH absorptivity (α in cm^{-1}) which is calculated using

$$\alpha = \frac{-\ln(T_{3000}/T_{5000})}{t}, \tag{1}$$

where T_{3000} and T_{5000} are the transmissions at 3000 and 5000 cm^{-1} wave numbers, respectively, and t is the thickness of the sample (cm). T_{5000} serves as a background transmission and includes the Fresnel reflection losses.

We profiled the OH content near the original exposed surface of the glass, using the following procedure. The exposed surface was ground with SiC emery paper to remove between 10–200 μm depending on the resolution desired and then polished first with 3 μm and then 1 μm diamond paste using a polishing oil (not water) as a lubricant. From the sample density and change in sample weight we determined the glass thickness removed. The OH absorptivity was re-measured using the FTIR spectrometer, and the absorptivity of the layer removed ($\alpha_{\Delta t}$) was computed using the following expression

$$\alpha_{\Delta t} = \frac{\alpha_t \cdot t - \alpha_{t-\Delta t} \cdot (t - \Delta t)}{\Delta t}, \tag{2}$$

where Δt is the thickness of the glass removed, and α_t and $\alpha_{t-\Delta t}$ are the absorptivities at thickness t and $t - \Delta t$, respectively. This process was repeated by regrinding, polishing and re-measuring the absorptivity until about 1 mm of the surface of the sample was removed. The error in our OH absorptivity measurements ranges from ±4% to ±18% based on standard error analysis techniques [10]; the precision for the various measured quantities is as follows: thickness removed (±10 μm), weight difference ($\pm 2.5 \times 10^{-4}$ g) and optical transmission (±0.1%).

Determination of absolute OH concentration from the OH absorptivity of the sample depends on the value of the extinction coefficient. However, reported values for the extinction coefficients at 3000 cm^{-1} vary from 30 [11] to more than 100 ppmw/cm^{-1} [12]. For this study, an extinction coefficient of 100 ppmw/cm^{-1} is assumed.

3.3. Measurement of physical and optical properties of the laser glass

Thermal expansion of the glasses was measured using a dilatometer (Theta model 7214) and heating cylindrical samples (5-mm diameter × 50-mm length) at a rate of 2°C/min from 20°C to a temperature just above T_g. Glass density was determined using the standard buoyancy method [13]. Fracture toughness was measured using both the Vickers indentation [14] and the chevron–notch [15] techniques. Vickers indentation measurements were carried out using a hardness testing machine (Zwick Werkstoff-Prüfmaschinen model 3212) on the polished surface of a $10 \times 10 \times 3$ mm^3 glass sample. Typically, a 0.6 kg load was applied to the glass surface for 15 s; the surface was covered with hexane to prevent moisture enhanced sub-critical crack growth. Details of the chevron–notch method are described elsewhere [15]. Refractive index and dispersion were measured using a custom built V-block refractometer [16]. Young's modulus and Poisson's ratio were determined in the standard fashion from measured acoustic velocities in the glass [17].

3.4. Preparation of glass laminates

Test samples $25 \times 25 \times 10$ mm^3 were cut from each glass melt (A–F) and then one surface (25×25 mm^2) of each test sample was lightly ground using 600 grit emery paper and water. Next, the ground surface of each of the glasses A–F was placed in contact with the ground surface of glass sample A forming a bilaminate. There were a total of six different bilaminate samples (A–A through A–F). The samples were fused together by heating the bilaminates to 570°C (∼100°C above T_g) for one hour. The fused laminates (which we call fusion samples) were cooled to 500°C in about 40 min. This was followed by a controlled 48°C/h ramp to 300°C and an uncontrolled cooling ramp (∼100°C/h) from 300°C to room temperature (i.e. power was removed from the annealing furnace). The joined fusion parts were then cut and polished on each side so that inspection could be conducted in a direction parallel to the fused surface. The final sample thickness in the inspection direction was 5 mm. The maximum stress birefringence in each fusion sample was measured using an optical microscope equipped with crossed polarizers and a compensating plate [18].

4. Results

4.1. OH concentration profiles near glass surface

Fig. 1 shows the measured OH profiles near the top surface of two identical meta-phosphate glass specimens (LG-770) subjected to the same annealing cycle but different ambient air environments. Both samples were annealed at <10°C/h from near T_g (~450°C) to 20°C but in one case the ambient air contained water vapor at a pressure of 7 mmHg and in the other case 17 mmHg. In both cases, the hydroxyl concentration is greater near the surface than in the interior, however at equivalent depths, the OH content is greater for the glass annealed in the air having the greater water vapor pressure.

4.2. Effect of OH content on glass properties

The effect of OH content on the thermal, mechanical and optical properties of LG-770 glass was determined using six glass samples with different OH contents (see Table 1). The OH content in the samples is expressed in terms of the optical absorption at 3333 nm (i.e. 3000 cm^{-1}) and ranges from 0.8 to 50 cm^{-1}; this corresponds to about 80 to 5000 ppmw OH, respectively.

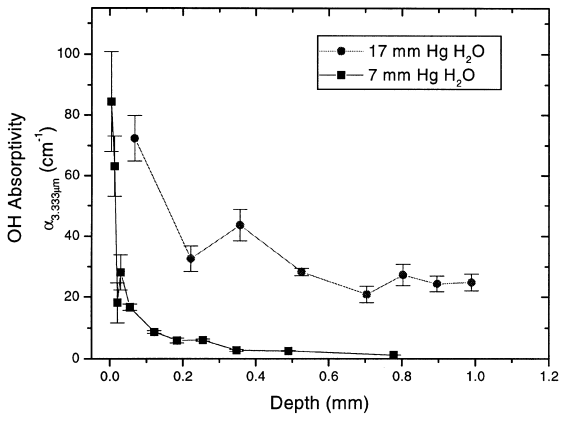

Fig. 1. Measured OH concentration as a function of the depth from the top surface for two LG-770 laser phosphate glasses annealed in air containing water vapor at pressure of 7 and 17 mmHg. The lines connect the data points.

Two key properties effected by glass OH content are the coefficient of thermal expansion (CTE) and the T_g (Fig. 2). Specifically, T_g decreases linearly by 63°C over the range of OH content investigated here. This decrease parallels the trend reported for silicates [12]. The CTE also increases approximately linearly with increase in OH content (Fig. 2). In contrast, Young's modulus (E) and Poisson's ratio (v) remain essentially constant over the range of OH contents reported here, with $E = 47$ (±1) GPa and $v = 0.26$ (±0.005) (Table 1). Also, the affect of OH content on the optical properties, such as the refractive index and the Abbe number, is negligible (Table 1).

The change in glass fracture toughness versus OH content was found to depend on the measurement technique. Fracture toughness measured by the chevron–notch technique showed no change with OH content to within the error of the measurement, however with the indentation technique a decrease in the fracture toughness with increase OH content was observed. The reason for this is not completely clear; however, we propose that samples measured using the indentation technique are more prone to stress-corrosion fracture (i.e. sub-critical crack growth) due to the presence of OH in the glass. Recent measurements of subcritical crack growth in phosphate laser glass showed that crack velocities increased with an increase in the OH content in the glass [8].

4.3. Stress birefringence measurements

The results of stress birefringence measurement on the six bilaminates (i.e. fusion samples) are summarized in columns 3 and 4 of Table 2. The stresses were estimated from the stress-induced birefringence, using a stress-optic coefficient of 21 nm/cm per MPa [7]. The stress-optic coefficient is not a function of residual OH content in LG-770; two samples with 3333 nm absorption coefficients differing by more than a factor of 100 (i.e. 0.6 and about 100 cm^{-1}) were both measured to have a stress-optic coefficient of 21 (±8%) nm/cm per MPa.

The stresses listed in Table 2 for the fusion laminates represent the maximum tension near the bond (fusion) interface. The peak tensile stress

Table 1
Effect of OH content on the properties of the meta-phosphate laser glass, LG-770, used in this study[a]

Property	Symbol	Units	Error	Sample designation					
				A	B	C	D	E	F
OH absorptivity at 3333 nm	$\alpha_{3.333\ \mu m}$	cm^{-1}	±0.4%	0.8	1.6	10.6	21.4	24.2	50.1
Thermal									
Softening Pt	T_{sp}	°C	±5	566	562	547	548	531	524
Glass Transition temp.	T_g	°C	±5	468	460	440	439	414	405
Linear expansion coefficient[b]	CTE	$\times 10^{-7}/K^{-1}$	±0.5	129	130	131	130	136	142
Mechanical									
Young's modulus	E	GPa	±1	48	47	47	48	47	47
Poisson's ratio	v		±0.005	0.259	0.260	0.259	0.258	0.260	0.260
Fracture toughness[c]	K_{Ic}	MPa $m^{1/2}$	±0.02	0.57	0.56	0.45	0.48	0.44	0.38
Fracture toughness[d]	K_{Ic}	MPa $m^{1/2}$	±0.02	0.43	0.45	0.43	0.44	0.43	0.43
Density	ρ	g/cm^3	±0.02	2.64	2.63	2.63	2.62	2.63	2.62
Optical									
Refractive index (587.6 nm)	n_d		±0.00002	1.51225	1.51184	1.51070	1.51270	1.50902	1.51067
Abbe number	v_d		±0.02	67.45	67.30	67.44	67.63	67.67	67.69

[a] LG-770 molar composition: (58–62)P_2O_5–(6–10)Al_2O_3–(20–25)K_2O–(5–10)MgO–(0–2)Nd_2O_3.
[b] Value from 20–300°C.
[c] Measured by Vickor's indentation method [14].
[d] Measured by chevron–notch method [15].

generally increases with an increase in difference between the OH content of the two laminated glasses. Based on repeated measurements, the standard deviation for measured stress at the bondline is <±15%.

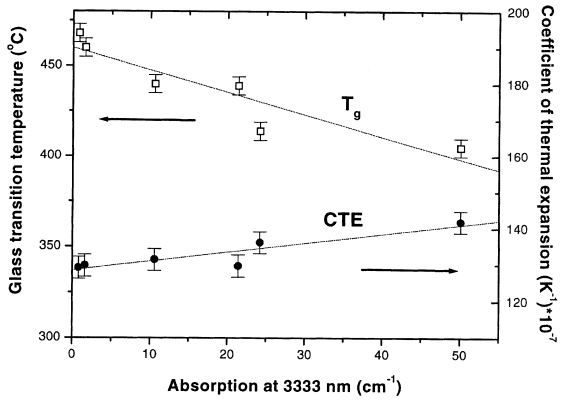

Fig. 2. Effect of OH content on the glass transition temperature (T_g) and the coefficient of thermal expansion (CTE) of LG-770 laser phosphate glasses. The lines are from linear regression analyses of the data.

Despite repeated trials, all fusion samples prepared using samples of glasses A and E and A and F broke during cutting and polishing of inspection samples. Analysis of the fracture patterns indicated high tension at the fusion join for these samples (see Table 2).

5. Discussion

5.1. Hydroxyl diffusion into the glass

The presence of a much greater OH content near the surface versus interior of the as-cast glass is not surprising because phosphate glasses are generally hygroscopic [19]. The external water vapor reacts with the linear metaphosphate chains at the surface of the glass to form chain terminating hydroxyl groups [1,12,20]

Table 2
Results from fusion bonding tests and FEA model calculations of glass A with other glasses having different OH contents

Glass sample fusion bonded to sample A	OH content $\alpha_{3.333\ \mu m}$ (cm^{-1}) (±0.4%)	Measured birefringence (nm/cm)	Implied stress (MPa) σ_{XX}	Net strain from thermal expansion curves $(\Delta L/L) \times 10^{-6}$ (±5%)	FEA predicted stress (MPa) σ_{XX}
A	0.8	2.0 ± 0.5	<0.1	0	
B	1.6	37 ± 2	1.8 ± 0.1	−130	
C	10.6	220[a]	10.5[a]	−490	13
D	21.4	156 ± 20	7.5 ± 1	−460	
E	24.2	Fractured	Fractured	−700	
F	50.1	Fractured	Fractured	−690	20.6

[a] Two other samples fractured.

$$2\left(\begin{array}{c} O \\ \| \\ -P- \\ | \\ O^- \end{array}\right) \leftrightarrow H_2O + \begin{array}{ccc} O & & O \\ \| & & \| \\ P & -O- & P \\ | & & | \\ O^- & & O^- \end{array} \qquad (3)$$

Ambient air can have a wide range of water contents depending on weather conditions and the level of process plant humidity control. Typically, the ambient water vapor pressure can vary from about 2 to 20 mmHg (260–2600 Pa). During processing, water vapor can react at the glass surface forming OH groups that diffuse into the bulk glass.

The rate of diffusion of OH into LG-770 between 400–1000°C has been previously reported [21]. These data, given in terms of diffusion coefficients (D), can be represented using the relationship

$$D \cong D_0\, e^{-Q/RT}, \qquad (4)$$

where R and T have their usual meaning and D_0 and Q are the pre-exponential constant and activation energy, respectively, and have values of 2.2 ± 1.0 cm^2/s, and 141 ± 7 kJ/mol based on a linear regression analysis of the diffusion data. Thus, the OH diffusion coefficients in LG-770 at 400 and 1000°C are about 2.5×10^{-11} and 3.6×10^{-6} cm^2/s, respectively; note that these values are about two to three orders of magnitude greater than values observed in soda-lime silicate glass at the same temperatures [22]. It is important to recognize that the diffusion coefficients given by Eq. (4) are probably not those for hydroxyl-groups per se, but rather the modifier, H^+ [12]. In addition, it is believed that the diffusion is concentration dependent, with the diffusion coefficient increasing as the OH content in the glass increases [23].

The time (t') required for OH to penetrate a given distance into the glass at a given temperature can be estimated using [24]

$$t' \cong \frac{x^2}{2D}, \qquad (5)$$

where x is the penetration depth, defined as the depth where the OH concentration is half the surface concentration (i.e. $C(x)/C_0 = 0.5$) [24]. The measured OH penetration depth is about 0.5 mm in a typical laser glass slab annealed in air containing water vapor at a pressure of 17 mm Hg (see Fig. 1). At a typical annealing temperature of 500°C the diffusion coefficient is approximately 6.5×10^{-10} cm^2/s, and hence 22 days would be required to achieve a penetration depth of 0.5 mm. Exposure times in excess of 25 days are commonly used during the annealing of large phosphate glass slabs [1].

Note that the diffusion of OH into the glass (after H_2O reaction at the surface) is an accumulation of the diffusion events that occur for all the temperatures and times to which the as-formed slab is exposed. OH penetration can occur in short exposure times (minutes) at temperatures $T \gg T_g$, as for example during casting [1]. It can also occur at lower temperatures ($T < T_g$) when the diffusion coefficient is smaller but the exposure times are much longer (days) as, for example, during annealing [1].

5.2. Explanation for surface tensile stress development

In Section 4.2, we showed that OH incorporation in the laser phosphate glass affects some of the

properties of the glass, specifically the thermal expansion coefficient and T_g. In this section, we describe how differences in these two properties result in stress in our glass laminates.

In a linear elastic solid, the stress ($\vec{\sigma}$) is related to the net strain ($\vec{\delta}$) by

$$\vec{\sigma} = \overleftrightarrow{c}\vec{\delta}, \tag{6}$$

where $\vec{\sigma}$ and $\vec{\delta}$ are six component vectors and $\overleftrightarrow{c}$ is the 6×6 elastic stiffness tensor [25]. The first three components of the stress and strain vectors describe the principal stresses and strains; the last three values describe shear components. For isotropic solids such as glass, $\overleftrightarrow{c}$ is described by two independent elastic moduli.

Consider an example using the two test glasses, sample A (a low OH content glass) and sample F (a high OH content glass) and having glass transition temperatures of T_{gA} and T_{gF}, respectively. Assume the samples are fusion-bonded together by heating above temperature T_{gA}. At this point there is no strain in the material; the strain/stress develops as the glass is cooled. For simplicity we assume cooling rate is slow enough that the thermal gradients in the glass part are negligible.

The mechanism for strain development during cooling of a glass-to-glass laminate is illustrated in Figs. 3 and 4. Fig. 3(a) shows the measured shrinkage ($\Delta L/L$) for each of the two laminate glasses (samples A and F) that contain different OH concentrations and Fig. 3(b) shows the differential shrinkage between these two glasses. During cooling a net strain develops as the temperature drops below T_{gF}; the magnitude of the strain is determined from the magnitude of the differential shrinkage between the two glasses as shown in Fig. 3(b).

The net strain (δ) in the glass can be represented by the sum of two contributions

$$\delta = \delta_l + \delta_{nl}, \tag{7}$$

where δ_l is a linear contribution to the strain due to differences in the linear coefficient of expansion for the high and low OH containing glasses. The term δ_{nl} is the contribution due to nonlinear shrinkage and dominates the strain at temperatures just below T_g (see Fig. 3(b)). The sign convention used in Fig. 3 is such that positive

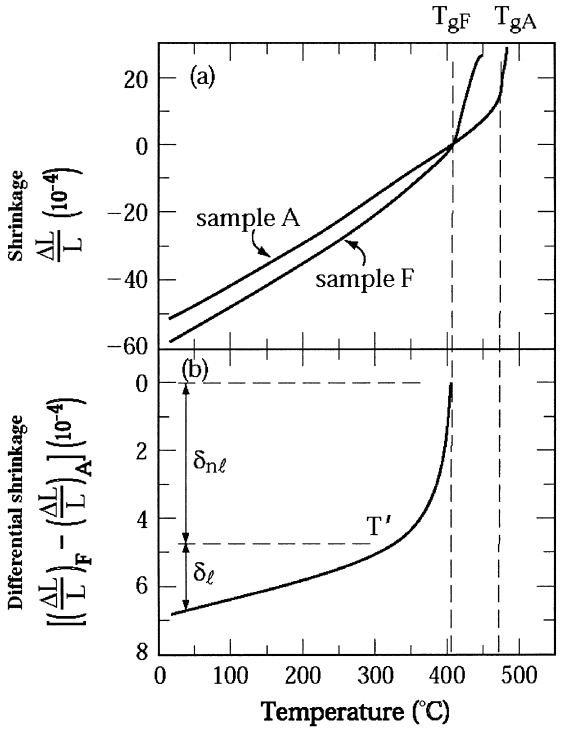

Fig. 3. (a) Dilatometer expansion curves of glass A (low OH) and F (high OH) (see Table 1) shifted to intersect at the glass transition temperature of the high OH glass (T_{gF}). (b) Differential shrinkage during cooling of a laminate (fusion sample) comprised of glass A and F. The differential shrinkage is calculated from the difference between the two curves in (a).

differential strains lead to tension, and negative strains result in compression.

Fig. 4 schematically illustrates strain development during cooling of a sample laminate comprised of two glasses (A and F) with different OH contents. When the laminated sample is above T_{gF}, the glass transition temperature of sample F, there is no stress because sample F relaxes viscoelastically to any differential shrinkage. When the laminate cools to temperature T_{gF}, the fusion join becomes stiff. At temperatures less than T_{gF}, the interface between the two glasses is constrained and stress develops as sample F shrinks more than sample A. The differential shrinkage between the two samples (A and F) is dominated by the nonlinear portion of the glass shrinkage until reaching temperature, T', and the net strain developed in this temperature range is labeled δ_{nl} (Fig. 4).

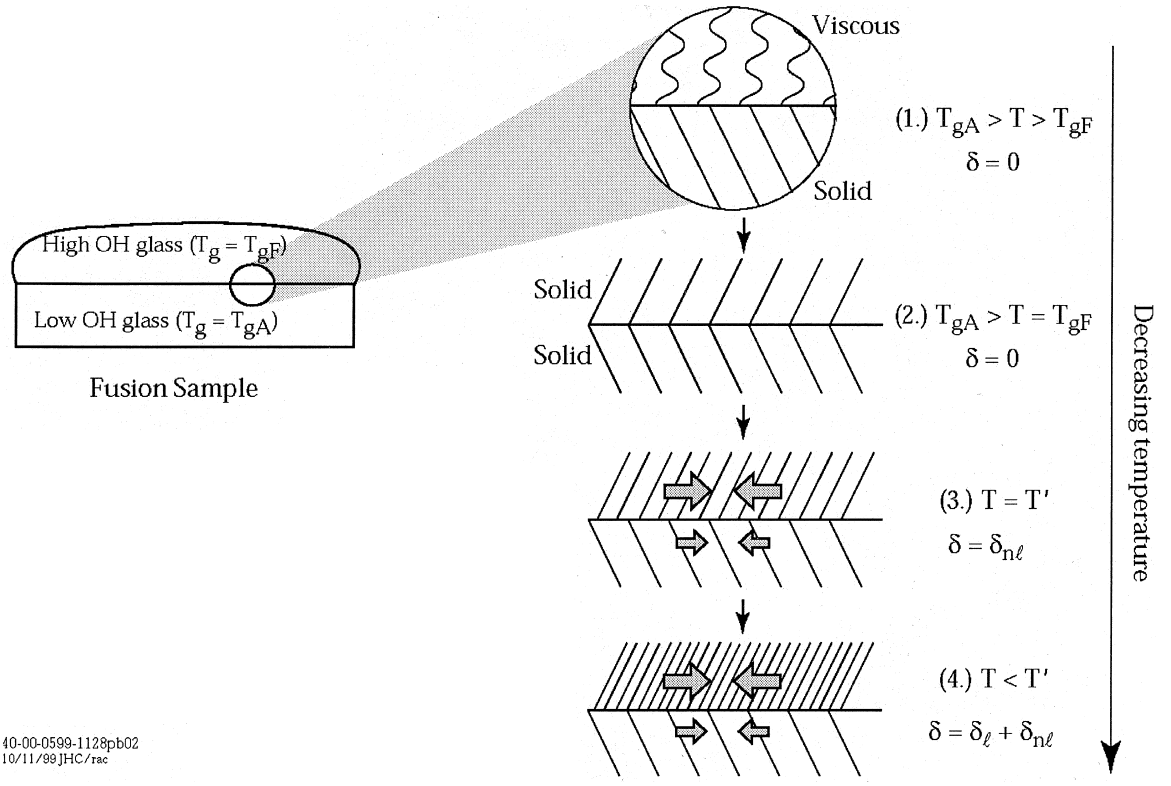

Fig. 4. Schematic illustration of the source of the differential shrinkage that develops during cooling of a fusion-bonded glass sample comprised of two glasses containing different hydroxyl contents.

Continued cooling below T' results in further differential shrinkage between the two samples, however in this region the shrinkage of both glasses is nearly linear with temperature and approximates the coefficient of thermal expansion. From the data in Table 1, the coefficient of linear thermal expansion is larger for the sample with the greater OH content, resulting in greater shrinkage of sample F relative to A and thus further increasing the net strain in the glass. The net strain continues to increase as the material is cooled to room temperature. The difference in shrinkage between the high and low OH content glasses produces a stress distribution near the fusion bond that is tensile in the high OH content glass and compressive in the low OH glass.

It is straightforward to estimate the net difference in linear shrinkage, δ_l, from the coefficient of thermal expansions, CTE_A and CTE_F, of sample A and sample F, respectively

$$\delta_l = (CTE_F - CTE_A)(T' - T_{RT}), \tag{8}$$

where T' is the temperature below which the thermal expansion coefficient is independent of temperature and T_{RT} is room temperature. Developing an analytical expression for δ_{nl} is more difficult since the theoretical relationship for the shrinkage near T_g is not known. Therefore, we determined δ_{nl} graphically for all six fusion samples from the dilatometer curves as shown in Fig. 3.

The total differential shrinkages (i.e. net strains (δ)) that develop during annealing of the six laminates are shown in Fig. 5. The data are plotted as a function of the difference in OH content between the two halves of the laminate. In general, the differential shrinkage increases with increasing difference in OH content between the two samples

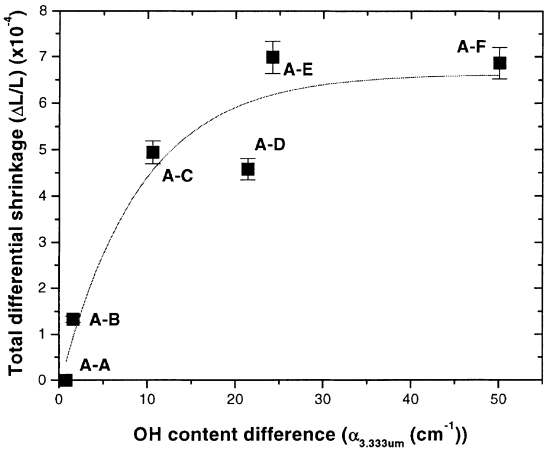

Fig. 5. Total differential shrinkage (strain) between two fusion-bonded samples having different OH contents; the strains were estimated from dilatometer curves as discussed in the text and in Fig. 3. The line does not represent a theoretical relationship but is drawn to illustrate the data trend.

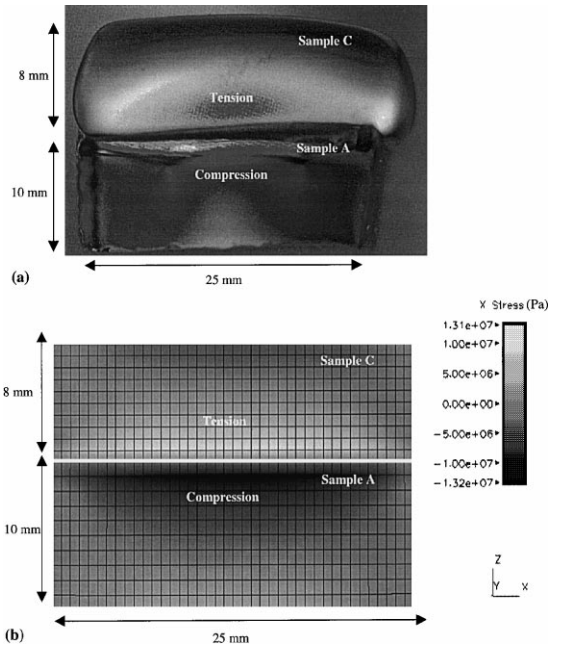

Fig. 6. (a) Photograph of fusion-bonded sample A–C with observed birefringence and (b) calculated stress distribution using a FEA model (via gray scale).

comprising the laminate. The differential shrinkage (net strain) varies from about 130 ppm in laminate sample A–B to about 700 ppm in samples A–E and A–F. Surprisingly, the total differential shrinkage appears to plateau at about 700 ppm at the highest differential OH content.

5.3. Calculated vs. measured stress

The peak tensile stress and stress distribution were calculated by FEA using the stress/strain code NIKE2D [26] and assuming the mechanism for strain development in the fusion samples as described in Section 5.2. The grid size and coordinate orientation used in the analysis is shown in Fig. 6. The calculations assume that the glass density (2.63 g/cm^3), elastic modulus (47 GPa) and Poisson's ratio (0.26) are unaffected by OH content in the glass, as reported in Table 1. As input, the FEA analysis uses the measured thermal expansion curves for the two samples in the bilaminate. Output from the FEA gives both the stress and strain distribution in the fusion sample. The simulations were carried out on two fusion samples; fusion samples A–C and A–F. As expected, the maximum tensile stress is computed to be near the fusion bond and just inside the sample with the greater OH content. The predicted stress profile through the fusion sample A–C is shown in Fig. 6 and visually compared with the observed birefringence in the sample. The calculated maximum tensile stress is +13 MPa for sample A–C which is close to the measured value of 10.5 MPa, based on the measured stress birefringence (see Table 2). The maximum tensile stress predicted by FEA for fusion sample A–F is 20.5 MPa; unfortunately, stress birefringence measurements could not be carried out on this sample because it fractured. The fact that sample A–F fractured means the stress (σ) exceeded the critical stress which depends on the glass fracture toughness (K_{IC}) and the critical flaw size a_c [27]:

$$a_c = \frac{1}{\pi}\left(\frac{K_{IC}}{\sigma}\right)^2. \tag{9}$$

Using Eq. (9) we estimate the critical flaw size of only 140 μm needed to produce failure at 20.5 MPa tensile stress. The occurrence of such a small flaw is not unreasonable.

5.4. Surface tensile stress generation and fracture in laser glass slabs

Using the strain data from the fusion samples, we can estimate the surface tensile stress in a typical phosphate laser glass slab that is annealed from a temperature slightly above T_g (~500°C) to room temperature. We assume that the glass is a laminate comprised of a 60-mm-thick core [with properties the same as those of sample A (see Table 1)] plus top and bottom surface layers 2-mm-thick and having properties the same as sample E. The stress at the core (σ_c) and surface (σ_s) for a part with this geometry are given by [25]

$$\sigma_c = \frac{-\delta E_s}{1-v}\left(\frac{a}{2c}+\frac{E_s}{E_c}\right)^{-1}, \tag{10}$$

$$\sigma_s = \frac{\delta E_c}{1-v}\left(\frac{2c}{a}+\frac{E_c}{E_s}\right)^{-1}, \tag{11}$$

where E_c and E_s are Young's moduli of the core and surface material, respectively, v is a composite Poisson's ratio, and a and c are the thickness of the surface and core glass, respectively. Since Young's modulus and Poisson's ratio do not vary with OH content, we assume $E_s = E_c \cong 47$ GPa and $v = 0.26$. Also, we assume the average OH concentration of the surface glass is about 3000 ppmw (i.e. 30 cm^{-1} absorption at 3.333 μm) based on measurements on annealed slabs. The expected net strain between the core glass and surface layers is about 700 ppm based on the difference in OH content (Fig. 5). Using Eqs. (10) and (11) we calculate a tensile stress of 42 MPa in the surface glass and less than −2.7 MPa compression in the thicker core plate. These values are consistent with our observations of tensile stresses near the slab surfaces of ~20 MPa based on measured stress birefringence. Stresses in slabs with OH contents greater than 30 cm^{-1} at the surface have not been made because in all cases these slabs fractured.

Based on the estimated tensile stress, Eq. (9) can be used to calculate the minimum flaw size (a_c) required to initiate fracture at the slab top surface [27]. Assuming a fracture toughness, K_{IC}, based on the chevron–notch measurements, the minimum flaw size to initiate fracture is 32 μm. With such a small flaw size, fracture is very likely to occur from minor defects or imperfections on the surface of the slabs in agreement with our observations.

Note that the above calculations are only approximate for the purpose of providing an estimate of surface stresses in phosphate laser slabs annealed in ambient air containing various concentrations of water vapor. The stress distribution in real production slabs is more complex for several reasons. First, the OH content is not constant over a given depth as assumed in the above calculation. Instead the OH content decreases with depth from the surfaces (as in Fig. 1) and therefore the stress developed will also decrease with depth. Second, the resistance to sub-critical crack growth also decreases with increasing OH content [8] resulting in a greater tendency for the glass exposed to water vapor during annealing to generate surface fractures. Finally, any tensile stresses that form due to the chemical modification of surface are in competition with the permanent compressive stress that is formed from thermal gradients in the glass during cooling. Nevertheless, the above simple calculation of surface tensile stress development during annealing of phosphate slabs gives a good approximation to our observations.

6. Conclusions

Tensile surface stresses and surface fractures have been observed after annealing slabs of metaphosphate laser glass in an ambient air containing water vapor. This is in sharp contrast to compressive surface layers generated during annealing of soda-lime silicate glasses under the same conditions.

Metaphosphate glasses have a chain-like structure consisting of PO_4 tetrahedra. Water vapor in the ambient air of the annealing oven can chemically attack phosphate glass surfaces, cleaving P–O–P chains and leaving behind shorter chains that terminate in hydroxyl groups. As a result of such attack, the glass surfaces take on properties different from the interior of the material, including an increase in thermal expansion and a decrease of the glass transition temperature. Changes in these two properties cause the slab

surface to shrink more during cooling than the interior, leading to castings with surfaces under tension. If suitable nucleation sites exist on the glass surface, this tensile layer can lead to a network of shallow surface cracks and, in extreme cases, catastrophic fracture of the slab.

To eliminate possible fracture problems associated with these surface stresses one must take steps to reduce or exclude water vapor from the annealing environment or at the end of the annealing cycle, immediately remove or pacify the stressed surface layer.

Acknowledgements

The authors gratefully acknowledge the contributions of R. Steele (OH profiles) and W. Miller (FEA modeling). This work was performed with funding provided by the US Department of Energy by Lawrence Livermore National Laboratory under Contract No. W-7405-Eng-48. The assistance of A. Flammini and A. Clasen in the preparation of the manuscript is deeply appreciated.

References

[1] J. Campbell, T. Suratwala, C. Thorsness, J. Hayden, A. Thorne, J. Cimino, A. Marker, K. Takeuchi, M. Smolley, G. Ficini-Dorn, these Proceedings, p. 342.
[2] J. Campbell, T. Suratwala, these Proceedings, p. 318.
[3] J. Murray, SPIE 3492 (1998) 1.
[4] M. Andre, M. Novaro, D. Schirmann, Chocs. Rev. Sci. Techn. Direct. Appl. Milit. 13 (1995) 73.
[5] F.V. Tooley, The Handbook of Glass Manufacture, vol. II, Ashlee, New York, 1984, p. 801.
[6] V.D. Frechette, Failure Analysis of Brittle Materials, vol. 28, American Ceramics Society, 1990.
[7] Glass for Laser Applications, Schott Glass Technologies, Product Catalog, Duryea, PA, 1999, p. 1.
[8] T.I. Suratwala, R.A. Steele, G.D. Wilke, J.H. Campbell, K. Takeuchi, these Proceedings, p. 213.
[9] D. Sapak, J. Ward, J. Marion, SPIE 970 (1988) 107.
[10] D.A. Skoog, J.J. Leary, Principles of Instrumental Analysis, 4th Ed., Saunders College Publishing, Orlando, FL, 1992.
[11] H. Toratani, PhD thesis, Kyoto University, Kyoto, 1989.
[12] J. Shelby, Handbook of Gas Diffusion in Solids and Melts, ASM International, Materials Park, OH, 1996, p. 217.
[13] Annual Book of ASTM Standards, 15.02, C-693-93 (1998) 213.
[14] B. Lawn, Fracture of Brittle Solids, 2nd Ed., Cambridge University, Cambridge, 1993.
[15] K.P.R. Reddy, E.H. Fontana, J.D. Helfinstine, J. Am. Ceram. Soc. 71 (1988) C310.
[16] J.V. Hughes, J. Sci. Instrum. 18 (1941) 234.
[17] A.K. Varshneya, Fundamentals of Inorganic Glasses, Academic Press, Boston, MA, 1990, p. 164.
[18] A. Ehringhaus, Z. Kristallogr. 76 (1931) 315.
[19] J.V. Wazer, Phosphorus and its Compounds, New York, 1958.
[20] R.M. Wenslow, K.T. Mueller, J. Phys. Chem. B 102 (1998) 9033.
[21] J. Hayden, M. Tomozawa, S. Crichton, Lawrence Livermore National Laboratory Report, UCRL-ID-136007 (1997) 1.
[22] E.B. Shand, Glass Engineering Handbook, McGraw-Hill, New York, 1958.
[23] M. Tomozawa, Commun. Am. Ceram. Soc. (Sept. 1985) C251.
[24] P. Atkins, Physical Chemistry, 5th Ed., Freeman, Oxford 1994.
[25] A.K. Varshneya, Treatise on Materials Science and Technology, Academic Press, New York, 1982.
[26] B. Engelmann, J.O. Hallquist, NIKE2D, A non-linear, implicit, two-dimensional finite element code for solid mechanics, Lawrence Livermore National Laboratory Report, UCRL-MA-105413, 1991.
[27] A. Griffith, Philos. Trans. R. Soc. A 221 (1920) 163.